Renewable Energy 229 (2024) 120782

Contents lists available at ScienceDirect

Renewable Energy

journal homepage: www.elsevier.com/locate/renene

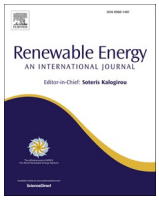

Experimental evaluation of the performance of new Copenhagen solar cooker configurations as a function of solar altitude angle

Xabier Apaolaza-Pagoaga [a,*], Antonio Carrillo-Andrés [a], Juan-Pablo Jiménez-Navarro [a], Celestino Rodrigues Ruivo [b,c]

[a] Energy Research Group. Department of Mechanical, Thermal and Fluids Engineering, University of Malaga. Calle Arquitecto Francisco Peñalosa, 6, 29071, Malaga, Spain
[b] Department of Mechanical Engineering, Institute of Engineering, University of Algarve, Campus da Penha, 8005-139, Faro, Portugal
[c] ADAI, Department of Mechanical Engineering, Rua Luís Reis Santos, Pólo II, 3030-788 Coimbra, Portugal

ARTICLE INFO

Keywords:
Solar cooking
Copenhagen cooker
Experimental test
Test without load
Water load test
Solar energy

ABSTRACT

The Copenhagen cooker is a panel-type solar cooker that uses four flexible reflective panels to redirect solar radiation to a cooking vessel. Its concept design allows adjustment of the four panels to create new geometries that can adapt to the solar altitude angle. Originally, three geometrical configurations were presented by its creators. In this work, building upon these originals, new configurations are proposed to improve performances. To quantify performance improvement, experimental tests are performed. First, stagnation tests are carried out to identify the best configuration for different solar altitude angles. Then, the most promising new configurations and the original ones are tested, side-by-side, heating a water load and for different ranges of altitude angle: low (35°), medium (66°) and high (75°). Results show that performance significantly improves. Results across the entire solar altitude angle range help general users to set the most effective configuration based on their specific conditions. Last, our experimental study suggests that tests without load can be a good predictor of the behaviour of solar cookers with load. This qualitative conclusion would allow solar cookers to be tested in shorter periods for all ranges of solar altitude angle, which is of great value for general users.

1. Introduction

Solar cooking holds significant potential for reducing the environmental impact associated with cooking activities that still largely rely on fossil fuels, i.e., in Europe, 96 % of final energy consumption for cooking comes from fossil fuels [1].

Given the possibilities offered by solar cooking, multiple solar cooker systems have been developed in the past years [2,3]. Common and simple solar cookers are usually classified as box, parabolic, panel and evacuated tube cooker types.

Many research works have focused on the characterisation of these different cooker designs [4–7], cooker configurations [8] and operational conditions [9–14] in order to determine their adequacy for specific cooking food applications.

In this work, the authors aim to investigate, extending the results presented in a previous work on the characterisation of the Copenhagen solar cooker [8], the performance of new design configurations taking advantage of the flexibility provided by its concept design.

The Copenhagen solar cooker is a panel type solar cooker designed in 2009 by Sharon and Glenn Clausson [15]. It is commercially available, and its design is open source. This, combined with its simple design, means that anyone can build their own Copenhagen cooker with widely available materials. It consists of four light-reflective surfaces that can be assembled in diverse ways to achieve different values of solar radiation collecting area and that can be adapted to the specific requirements of the food to be cooked, the cooking time, the amount of food, and operational conditions such as solar radiation availability or sun position during the cooking period. The set of reflectors of a Copenhagen solar cooker is lightweight, which is an aspect important for the user that are using the cooker in different contexts, i.e., not only at home in a fixed place. Moreover, the shipping costs are relatively low.

In a previous work [8], authors assessed the three original configurations proposed by its designers namely *Cave*, *Ninety* and *Flower*, and made recommendations on how to use them according to the solar altitude angle range.

Here, authors propose new reflector configurations that are tested to evaluate their performance. With these new designs, the authors aim to

* Corresponding author.
E-mail address: apaolaza@uma.es (X. Apaolaza-Pagoaga).

https://doi.org/10.1016/j.renene.2024.120782
Received 22 November 2023; Received in revised form 24 May 2024; Accepted 6 June 2024
Available online 11 June 2024

Nomenclature

$A_{n,max}$	Maximum area normal to the incoming beam irradiation collected by the solar cooker (m^2)
C_g	Cooker geometric concentration ratio (−)
$c_{p,w}$	Specific heat of load (J kg^{-1} $°C^{-1}$)
F'	Heat exchange efficiency factor (−)
F_1	First figure of merit (m^2 °C W^{-1})
I	Global solar irradiance on a horizontal surface (Wm^{-2})
I_b	Beam irradiance on a horizontal surface (Wm^{-2})
I_{bn}	Beam normal solar irradiance (Wm^{-2})
$\bar{I}_{bn}$	Average beam normal solar irradiance during a test (Wm^{-2})
I_d	Diffuse solar irradiance on a horizontal surface (Wm^{-2})
I_n	Global normal solar irradiance (Wm^{-2})
$\bar{I}_n$	Average global normal solar irradiance during a test (Wm^{-2})
$I_{n,i}$	Global normal solar irradiance for a time interval i (Wm^{-2})
I_T	Total irradiance on the titled surface (Wm^{-2})
m_w	Mass of load (kg)
n_p	Number of valid points for plotting performance linear regression
$\dot{Q}$	Cooker power (W)
$\dot{Q}_i$	Cooker power at time interval i
$\dot{Q}_S$	Standardised cooker power (W)
$\dot{Q}_{S,0}$	Standardised cooker power for $\Delta T_{w,a} = 0$ °C (W)
$\dot{Q}_{S,50}$	Standardised cooker power for $\Delta T_{w,a} = 50$ °C (W)
R_b	Ratio of beam radiation on the titled surface to that on a horizontal surface
R^2	Coefficient of determination (−)
T_a	Ambient temperature (°C)
$\bar{T}_a$	Average ambient temperature for a testing period (°C)
$T_{a,pot}$	Temperature inside the pot in tests without load (°C)
T_{stag}	Stagnation temperature (°C)
T_w	Load temperature (°C)
U_L	Heat loss factor (W m^{-2} $°C^{-1}$)
$\bar{v}_a$	Average air velocity during a test (m s^{-1})

Greek symbols

α_s	Solar altitude angle (°)
$\bar{\alpha}_s$	Average solar altitude angle during a test (°)
$\alpha_{s,end}$	Solar altitude angle at the end of the test (°)
$\alpha_{s,noon}$	Solar altitude angle at solar noon (°)
$\alpha_{s,start}$	Solar altitude angle at the start of the test (°)
β	Slope angle of a surface to the horizontal surface (°)
γ	Surface azimuth angle, the deviation of the projection on a horizontal plane of the normal to the surface from the local meridian (°)
γ_s	Solar azimuth angle, the angular displacement from south of the projection of beam radiation on the horizontal plane (°)
$\Delta A_{n,max,new,original}$	Difference between areas normal to the incoming beam irradiation collected by the solar cooker of the new and original solar cooker configuration (m^2)
$\Delta \dot{Q}_{s,0,new,original}$	Difference between standardised cooker powers for $\Delta T_{w,a} = 0$ °C of the new and original solar cooker configuration (W)
$\Delta \dot{Q}_{s,50,new,original}$	Difference between standardised cooker powers for $\Delta T_{w,a} = 50$ °C of the new and original solar cooker configuration (W)
Δt_i	Duration of time interval i (s)
$\Delta T_{stag,s}$	Normalised stagnation temperature difference for solar irradiance of 1000 W m^{-2} (°C)
$\Delta T_{stag,s,new}$	Normalised stagnation temperature difference for solar irradiance of 1000 W m^{-2} of new solar cooker configuration (°C)
$\Delta T_{stag,s,original}$	Normalised stagnation temperature difference for solar irradiance of 1000 W m^{-2} of original solar cooker configuration (°C)
$\Delta T_{stag,s,new,original}$	Difference between normalised stagnation temperature differences for solar irradiance of 1000 W m^{-2} of new and original solar cooker configurations (°C)
$\Delta T_{w,a}$	Temperature difference between load and ambient (°C)
δ	Declination (°)
η	Instantaneous efficiency (−)
η_0	Optical efficiency (−)
η_{50}	Cooker efficiency for $\Delta T_{w,a} = 50$ °C (−)
θ	Angle of incidence, the angle between the beam radiation on a surface and the normal to that surface (°)
θ_z	Zenith angle, the angle of incidence of beam radiation on a horizontal surface (°)
ρ_g	Albedo (−)
φ	Latitude (°)
χ	Specific temperature difference (m^2 °C W^{-1})
χ_i	Specific temperature difference at time interval i (m^2°C W^{-1})
ω	Hour angle, the angular displacement of the sun east or west of the local meridian due to rotation of the earth on its axis, at 15° per hour (°)

Abbreviations

CCj	Copenhagen solar cooker, where j is a number to identify a particular unit being tested in parallel (j = 1, 2 and 3)

increase the potential of the Copenhagen solar cooker by setting up geometrical configurations providing better performance. To do so, the authors carried out an extensive experimental work including no-load stagnation tests and water heating tests for different ranges of solar altitude angle.

This paper is organised as follows: i) Section 2 includes the description of the new configurations as well as the experimental setup to measure all the variables that have an impact on their performance, ii) in Section 3, we continue explaining the tests performed including key modifications to the standardised testing procedure, iii) in Section 4, the results of the tests are presented and iv) a discussion and future research directions are addressed in Section 5.

2. Copenhagen solar cooker configurations and experimental setup

The Copenhagen solar cooker consists of four-square light-reflective panels of 368 mm by 368 mm, shown in Fig. 1 as S_a, S_b, S_c and S_d, and a square double layer wood plate of 203 mm by 203 mm. Each squared panel is made of self-adhesive polyester film that covers a polypropylene substrate sheet. The polyester film actuates as reflector. It is manufactured by General Formulations Inc. (www.generalformulations.com) with the product reference S2-STC-AP/90. The wood plate is placed over the four squared panels as shown in Fig. 1 and it forms the cooking area where pots or cooking vessels are placed. The reflective panels redirect the solar rays onto the cooking pot, as illustrated in Fig. 2.

To characterise the geometry of the new configurations tested in this

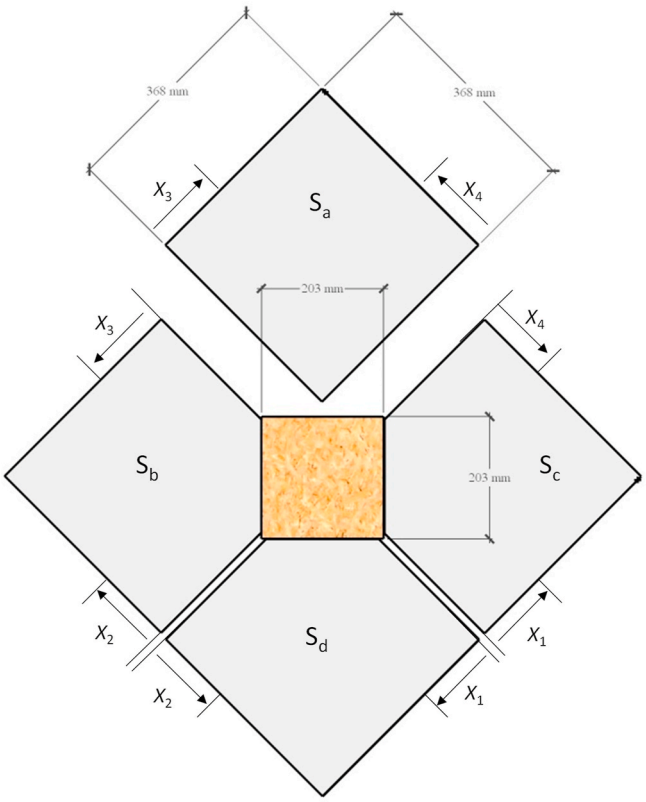

Fig. 1. Five-piece set of the Copenhagen solar cooker.

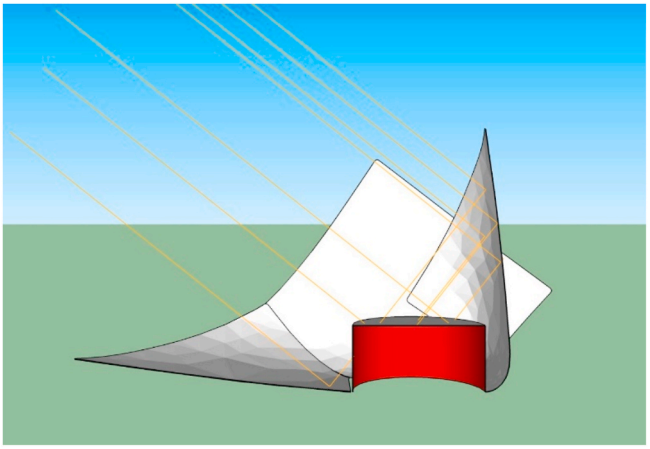

Fig. 2. Schematic drawing of the optical system of the Copenhagen cooker in Ninety configuration.

work, we have indicated the reference distances X_1 to X_4 shown in Fig. 1, which were measured from the joint line between two adjacent sheets toward their vertices. The values of these distances determine the connection points between adjacent sheets. In this way, X_2 sets the position of the screws that keeps together sheets S_c and S_b relative to their joint line.

Using these distances (X_1 to X_4), we define the new configurations to be experimentally assessed in this work. The six configurations investigated are depicted in Fig. 3 and are: i) *Medium* and *Big Flower,* ii) *Star* and *Square* as well as iii) the original *Flower* and *Ninety*, already evaluated by the authors, that serve as references to quantify performance improvements. Here, the *Cave* configuration is not considered due to its lower performance compared to the others as discussed by the authors in Ref. [8].

The rationale behind these new configurations is to explore configurations with larger aperture areas and compare them to the originals for a given set of conditions. In this work, the aperture area is defined as the maximum area normal to the incoming beam solar radiation collected by the solar cooker $A_{n,max}$. Due to the complex geometry of the configurations, this area is determined experimentally [16]. The procedure involves using the solar cooker, a camera and a rectangular frame as a reference for measurements. The solar cooker is placed at its designed position, i.e., horizontally (see Fig. 4) and within the frame. Then, the camera and the frame are set in complementary angles, which means that the camera faces the surface of the frame perpendicularly. Pictures are then taken for various angles of the camera and frame and for each angle the area of the cooker is computed using the dimension of the frame as a reference. From all the areas computed the maximum is determined. From a geometrical perspective, for the *Flower* configurations set, the aperture area values of the new *Medium flower* and *Big Flower* are 62 % and 104 % larger, respectively, to the original *Flower* at the expense of a probably lower interception ratio. The new *Star* configuration is a modification of the original *Ninety* with a larger aperture area of the side reflecting panels that increases the aperture area by one third. Last, the new *Square* configuration is built using two of the panels placed vertically and the other two horizontally, which represents a different geometrical arrangement. The three *Flower* configurations are intended for high solar altitude angles while the other configurations are better for medium and low solar altitude angles. It is important to note here that the four new configurations that are tested in this work have the same total reflective area of 0.542 m^2 (0.135 m^2 per squared light-reflective surfaces) as the original ones since they are built based on the same set of light-reflective surfaces. Distances X_1 to X_4 considered in each case and the corresponding maximum aperture area to the incoming beam normal solar radiation are presented in Table 1.

In each cooker, a set composed of a black pot with glass lid, inside a massive glass enclosure, used in a previous study [8], was adopted. The pot is made of steel with an enamel black layer. It has a maximum capacity of 3 L, diameter of 200 mm, a height of 100 mm, and a mass of 540 g. The glass lid of each pot has a mass of 366 g. The enclosure is composed of two glass washing machine windows, working as a greenhouse, where the pot is inserted. The mass of each transparent heat trap is approximately 2240 g, being the thickness approximately 5 mm.

In the experiments with loads, 1.5 kg of water were used, irrespective of the cooker configuration. Thus, the load ratio ranges from 3.74 kg m^{-2} in new *Big Flower* to 7.61 kg m^{-2} in original *Flower*. The recommended load ratio for the ASAE S580.1 standard is 7 kg m^{-2} [17].

The solar cookers were tested in the experimental facilities of the Energy Research Group at the School of Engineering of the University of Málaga, Spain at a latitude of 36.9° N. Tests were conducted from May to November 2021 and May to July 2022. Detailed data can be found in Appendix A.

Five T-type thermo-couples with a tolerance of ±1 °C were positioned 10 mm from the bottom of the pot. One sensor was placed at the centre of the pot and the positions of the other four additional sensors formed a square whose ends were all approximately 10 mm from the pot wall. The average temperature value of these five sensors provides a more robust measure of the temperature. A weather station, placed on the rooftop of the building and close to the experimental set-up, was used to measure the global, direct and diffuse solar irradiances on the horizontal plane, using a Delta-T Devices SPN1 pyranometer. From these measurements, the direct normal irradiance is calculated, using the Liu Jordan isotropic sky model [18]. Details on this calculation can be found in Appendix B. Additionally, two Hukseflux LP02 pyranometers located next to the solar cookers being tested were also used. One was placed horizontally and the other on a tilted plane with a slope of 40° to the horizontal plane. Azimuthal adjustments of the two pyranometers were performed every 20 min, i.e., at the same time the cookers were also adjusted azimuthally. This adjustment frequency is sufficient for low

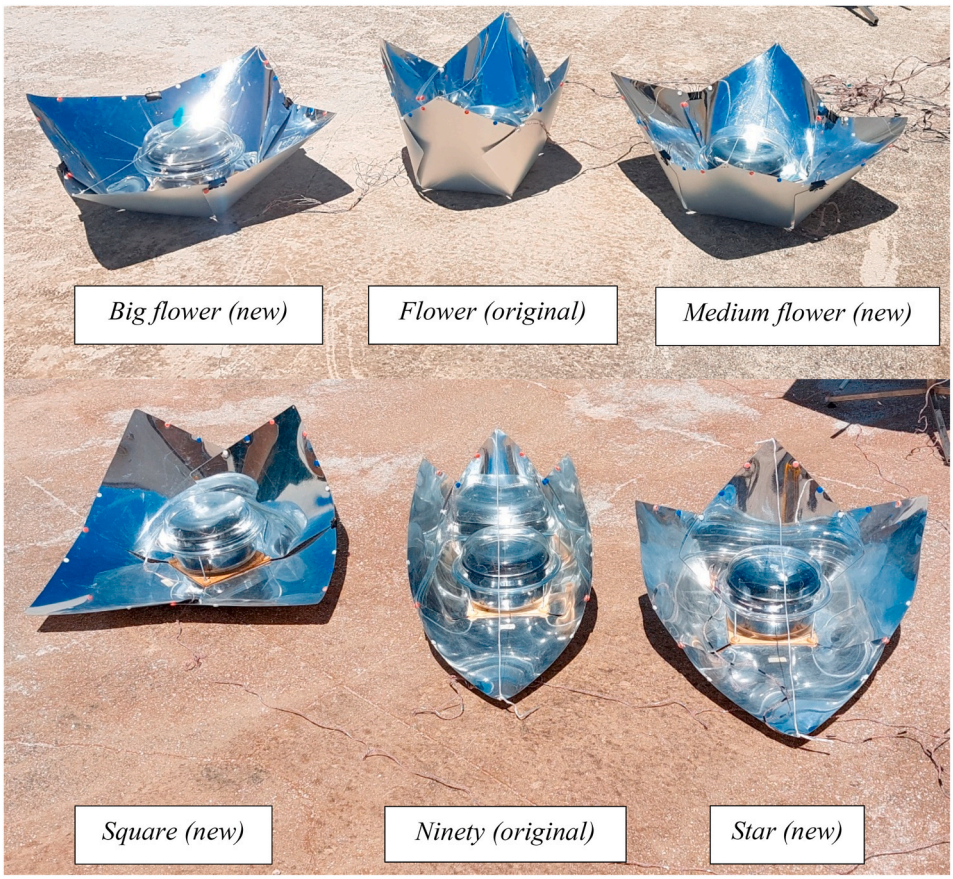

Fig. 3. Original and new Copenhagen cooker configurations.

concentration ratio devices. Measurements from these two pyranometers were used to verify irradiance calculations made with the SPN1 data and the Liu Jordan model. Details can be found in Appendix B. The measurements of the two LP02 pyranometers, and of several type T thermocouples, were recorded in a Campbell Scientific CR1000 data logger, every minute. Wind speed and ambient temperature were measured by a dedicated Onset weather station located near the solar cookers being tested. Measurement ranges and technical specifications of the instruments used are summarized in Table 2.

Fig. 4 depicts the experimental setup for testing three Copenhagen solar cookers simultaneously and the measuring devices both for the water load test and the stagnations tests, which are the two methods used in this work and explained in more detail in the coming section. Fig. 4a) shows three cookers being tested side by side in a test with load and Fig. 4b) shows two cookers being tested side by side in a test without load, where each cooker is placed on a tilted board with an inclination angle β to the horizontal plane.

3. Methods

In this work two testing procedures are adopted: no-load stagnation tests and water heating tests. The obtained results in these two tests allow a more comprehensive experimental characterisation of the cooker. By comparing both tests, conclusions can be drawn on how well the no-load stagnation tests can predict what configuration performs better when the cooker is in operation with a load. In this section, the main details of each test are explained.

3.1. Heating tests with a load

The water heating experiments test the ability of a solar cooker to heat up a certain amount of water placed in the vessel. The ASAE S580.1 Standard provides guidance on how to perform this analysis [17]. However, in a previous work [19], the authors identified methodological inconsistencies and proposed a modification to the data processing procedure of the standard. The formulation used here is consistent with the well-established Hottel-Whillier-Bliss formulation [18]. Accordingly, the rate of useful heat gain by water is expressed by:

$$\dot{Q} = A_{n,max} F' \eta_0 I_n - A_r F' U_L (T_w - T_a) \quad (1)$$

where $A_{n,max}$ is the maximum collecting area of the cooker, which is different for each geometrical configuration, and occurs for a specific solar altitude angle. The parameter η_0 is the optical efficiency, defined as the fraction of the incident solar radiation rate on the collecting area that is absorbed at the pot surfaces. The variable I_n refers to the global normal solar irradiance, i.e., the global solar irradiance measured on the plane perpendicular to the beam solar radiation. Geometrical losses due to the eventual misalignment between the direction of I_n and the normal of $A_{n,max}$ plane are included in the optical efficiency. The parameter A_r is the absorbing surface area of the pot, the variable U_L represents the heat loss factor, T_w the water temperature, T_a the ambient temperature and F' the heat exchange efficiency factor.

The instantaneous efficiency can be defined as the ratio of the useful heat rate gained by the load to the of solar radiation rate intercepted by the reflector if the reflector of solar cooker perfectly tracked or could tracked the sun at each instant, which means that in ideal tracking scenario the effective area of interception would be $A_{n,max}$:

$$\eta = \frac{\dot{Q}}{A_{n.max} I_n} \quad (2)$$

Combining Eqs. (1) and (2), the efficiency η can be expressed as:

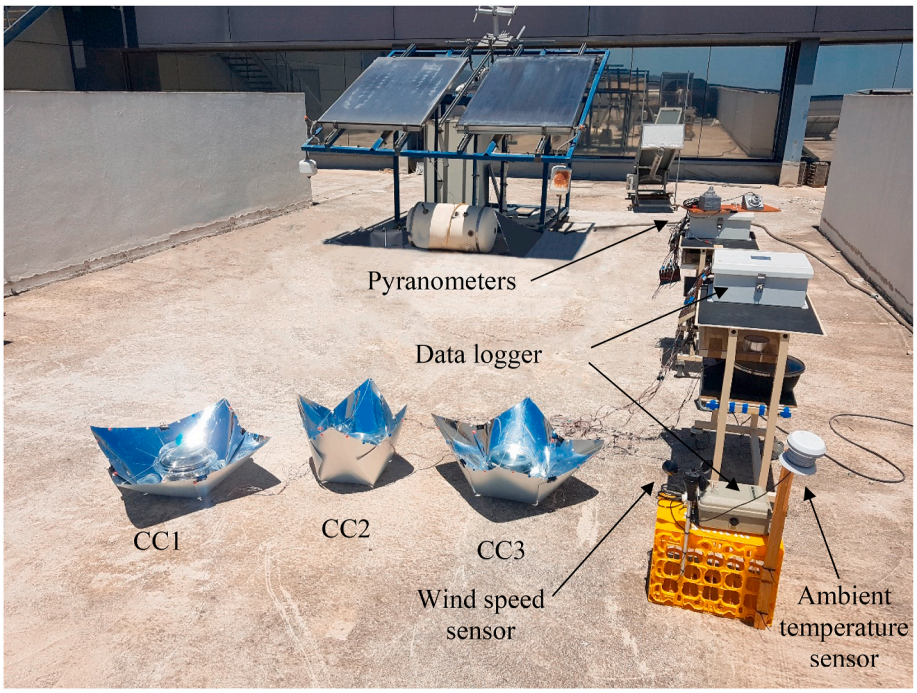

a)

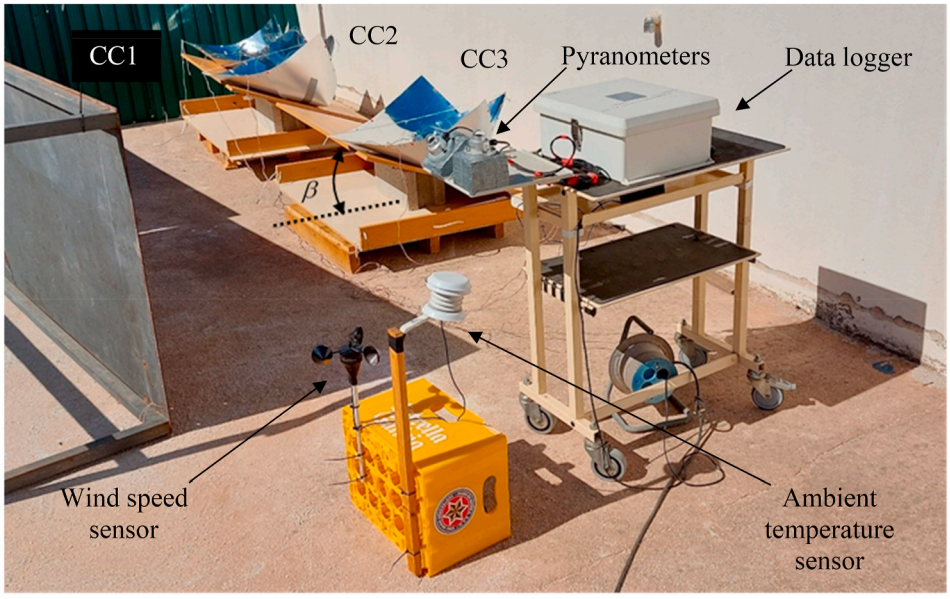

b)

Fig. 4. Experimental setup used for testing the solar cookers: a) water heating tests and b) tests without loads.

Table 1
- Distances X_1 to X_4 for the different cooker configurations.

Base design	Configuration	$A_{n,max}$ (m^2)	X_1 (mm)	X_2 (mm)	X_3 (mm)	X_4 (mm)
Flower	*Flower* (original)	0.197	115	115	115	115
	Medium flower (new)	0.320	60	60	60	60
	Big Flower (new)	0.401	40	40	40	40
Ninety	*Ninety* (original)	0.238	10	10	190	190
	Star (new)	0.317	10	10	115	115
	Square (new)	0.339	10	10	10	115

$$\eta = F'\eta_0 - \frac{F'U_L}{C_g}\chi \tag{3}$$

where the cooker geometric concentration ratio C_g and the specific temperature difference χ are expressed respectively by:

$$C_g = \frac{A_{n,max}}{A_r} \tag{4}$$

$$\chi = \frac{T_w - T_a}{I_n} \tag{5}$$

Table 2
- Instruments used to measure the solar irradiance, air speed and temperature.

Variable	Instrument	Operation range	Technical specifications
Global, direct and diffuse solar irradiance (W m^{-2})	SPN1 pyranometer (Delta-T Devices ltd)	0 to 2000	Overall accuracy: ±8 % ± 10 W m^{-2}
Global solar irradiance (W m^{-2})	LP02 pyranometer (Hukseflux)	0 to 2000	Calibration uncertainty <1.8 %
Air speed (m s^{-1})	3 cup anemometer *S*-WSB-M003 (Hobo Onset)	0 to 76	Accuracy: ±4 % of reading whichever is greater. Resolution: 0.5 m s
Ambient temperature (°C)	Thermistor *S*-TMB-M002 (Hobo Onset)	−40 to 75	Accuracy < ±0.2 from 0 to 50 °C
Water or air temperature inside pot (°C)	Thermocouple type T (TC Ltd)	−75 to 250	Tolerance: ±1.0 °C

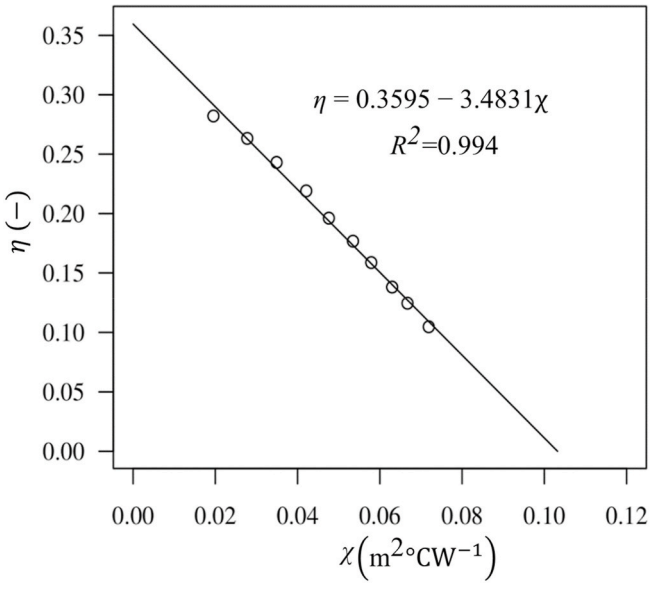

Fig. 5. Example of linear fit to determine the Hottel-Whillier-Bliss model parameters in test number 191 CC1.

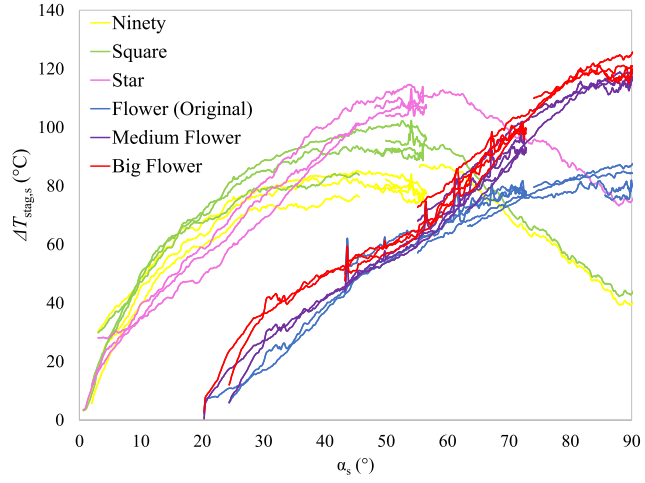

Fig. 6. Normalised stagnation temperature difference ($\Delta T_{stag,s}$) vs. solar altitude angle (α_s).

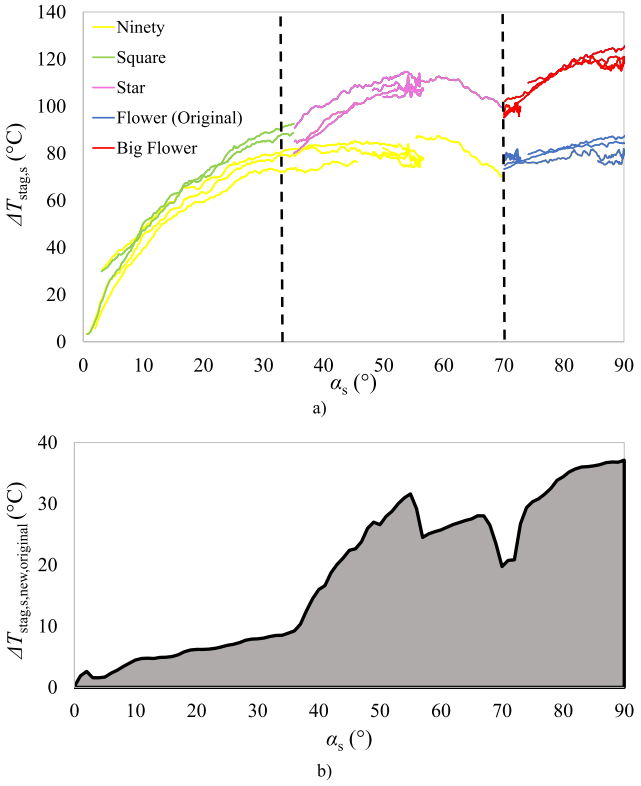

Fig. 7. Stagnation performance of original and new configurations along solar altitude angle: a) normalised stagnation temperature difference and b) increment of normalised stagnation temperature difference between the best new configuration and the best original configuration, for each solar altitude.

The useful gain rate is directly proportional to the rate of increase of the load temperature:

$$\dot{Q} = m_w C_{p,w} \frac{dT_w}{dt} \tag{6}$$

where m_w and $C_{p,w}$ are the mass and the specific heat of water, respectively. The experimental data is clustered in time intervals of 10 min. For each time interval i, the experimental data is used to calculate the value of efficiency η_i as $\frac{\dot{Q}_i}{A_{n,max} I_{n,i}}$ and the specific temperature difference χ_i as $\frac{T_{w,i} - T_{a,i}}{I_{n,i}}$. During a test, the main variations are observed in variable $T_{w,i}$. The variations of $T_{a,i}$ and $I_{n,i}$ must be relatively small. By plotting the n_p valid points (η_i, χ_i) for each time interval and performing a linear fit, the parameters $F'\eta_0$ (y-intercept) and $\frac{F'U_L}{C_g}$ (slope coefficient) can be estimated (Fig. 5).

Eq. (1) expressing the useful power of the cooker can be rewritten as:

$$\dot{Q} = I_n A_{n,max} F'^{\eta_0} - A_{n,max} \frac{F'U_L}{C_g} (T_w - T_a) \tag{7}$$

for the ternary I_n, T_w and T_a. If a standard global solar irradiance of 1000 W m^{-2} is adopted, the standardised power rate is expressed as:

$$\dot{Q}_S = 1000 A_{n,max} F'^{\eta_0} - A_{n,max} \frac{F'U_L}{C_g} (T_w - T_a) \tag{8}$$

The ASAE S580.1 Standard recommends a standard global solar irradiance of 700 W m^{-2}. In the present work, the value of 1000 W m^{-2} is adopted because, in the authors opinion, it better reflects the typical conditions of solar cooker operation during a clear sky day. Finally, the standardised power and the efficiency are reported for the point where the difference between the load temperature and ambient air ($\Delta T_{w,a}$) is equal to 50 °C, and denoted respectively by $\dot{Q}_{S,50}$ and η_{50}.

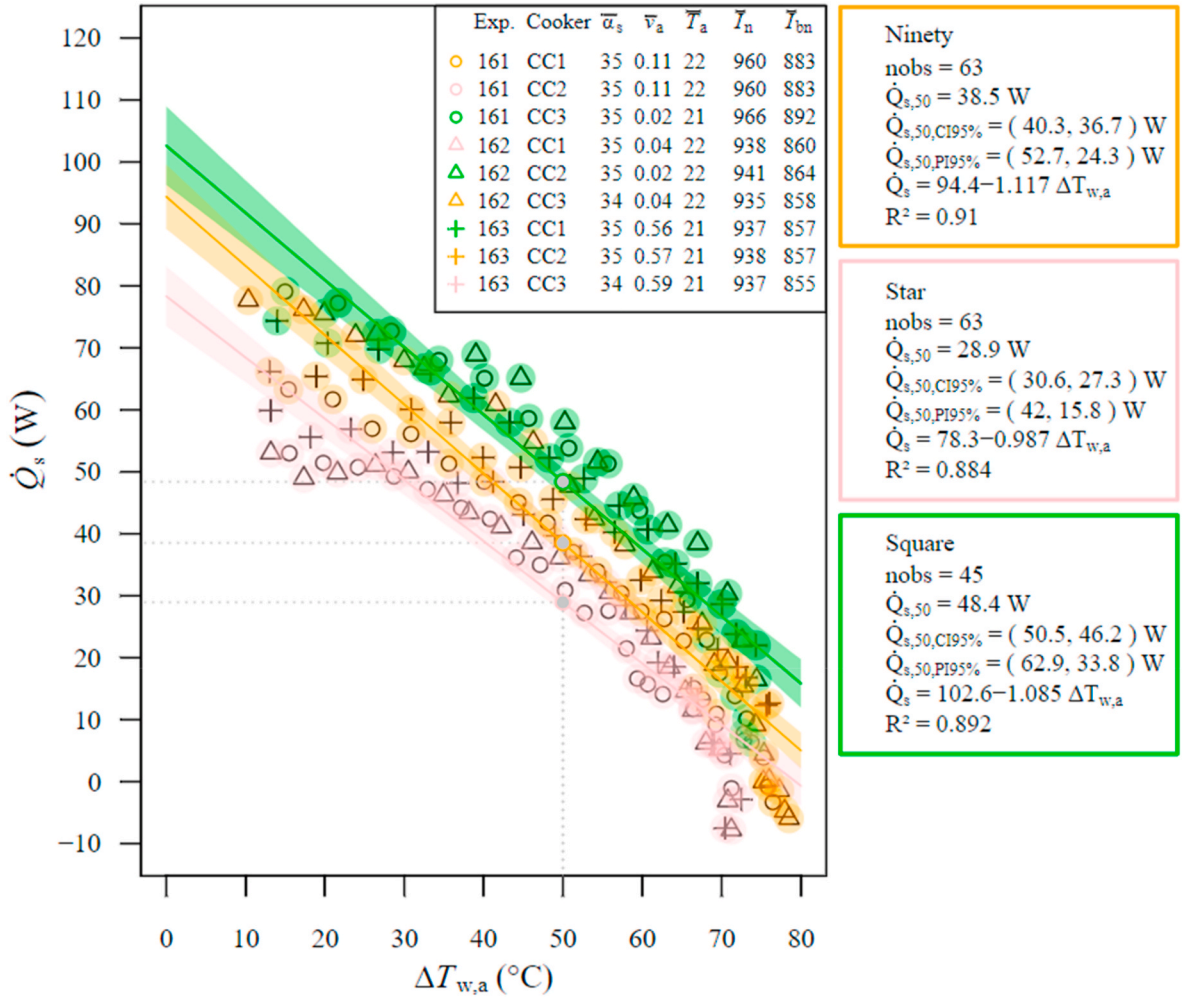

Fig. 8. Standardised power ($\dot{Q}_s$) vs. temperature difference ($\Delta T_{w,a}$) for low average solar altitude angle ($34° \leq \bar{\alpha}_s \leq 35°$) for the *Ninety*, *Star* and *Square* configurations.

3.2. Heating tests without load

Heating tests without load, i.e., no-load stagnation tests are performed with empty pots, i.e., the vessel only contains air. These tests allow identification of the optimal solar altitude angle range. Tilting boards (Fig. 4b) were used to emulate solar altitude angles that would be out of range for the particular location of Málaga (36.7° N). The cooker concentrator remains oriented in azimuth towards the sun, which in its trajectory changes its angle of elevation, which entails a modification of the optical efficiency of the solar cooker. This in turn modifies the temperature measured inside the pot. In practice, the difference between the temperature measured inside the unloaded pot and that of the environment, normalised with the incident solar irradiance, is a function only of the solar altitude angle and does not depend on the thermal history of the system. This is supported by the empirical observation that the mentioned magnitude is independent of whether the system evolves from a higher temperature at previous moments or, on the contrary, evolves from a lower temperature. Therefore, in practical terms, the temperature measured inside the pot can be seen as a stagnation temperature (T_{stag}). In this equilibrium condition, the following relationship is verified:

$$\frac{\eta_0 C_g}{U_L} = \frac{T_{stag} - T_a}{I_n} \tag{9}$$

Each term of Eq. (9) corresponds to the ratio of optical efficiency to heat loss factor, also known as the first figure of merit (F_1) in solar cooker testing literature [20]:

$$F_1 = \frac{\eta_0 C_g}{U_L} = \frac{T_{stag} - T_a}{I_n} \tag{10}$$

Analogously to the previous section, a normalised stagnation temperature difference ($\Delta T_{stag,s}$) can be defined, for a standard solar irradiance of 1000 W m^{-2}, as:

$$\Delta T_{stag,s} = 1000 F_1 \tag{11}$$

In this study, $\Delta T_{stag,s}$ is determined for solar altitude angles between 0° and 90° for each cooker configuration.

4. Results and discussion

In this section, the results of stagnation tests without load are presented first, followed by the results of the water heating tests.

4.1. Results of tests without load

The values of the normalised stagnation temperature difference $\Delta T_{stag,s}$ versus the solar altitude angle for the six analysed configurations are depicted in Fig. 6. Each curve represents an individual stagnation test (see Appendix A for detailed data). Results confirm that the *Ninety*, *Square* and *Star* cooker configurations, which were intended for low and medium solar altitude angles, show the best performance in these

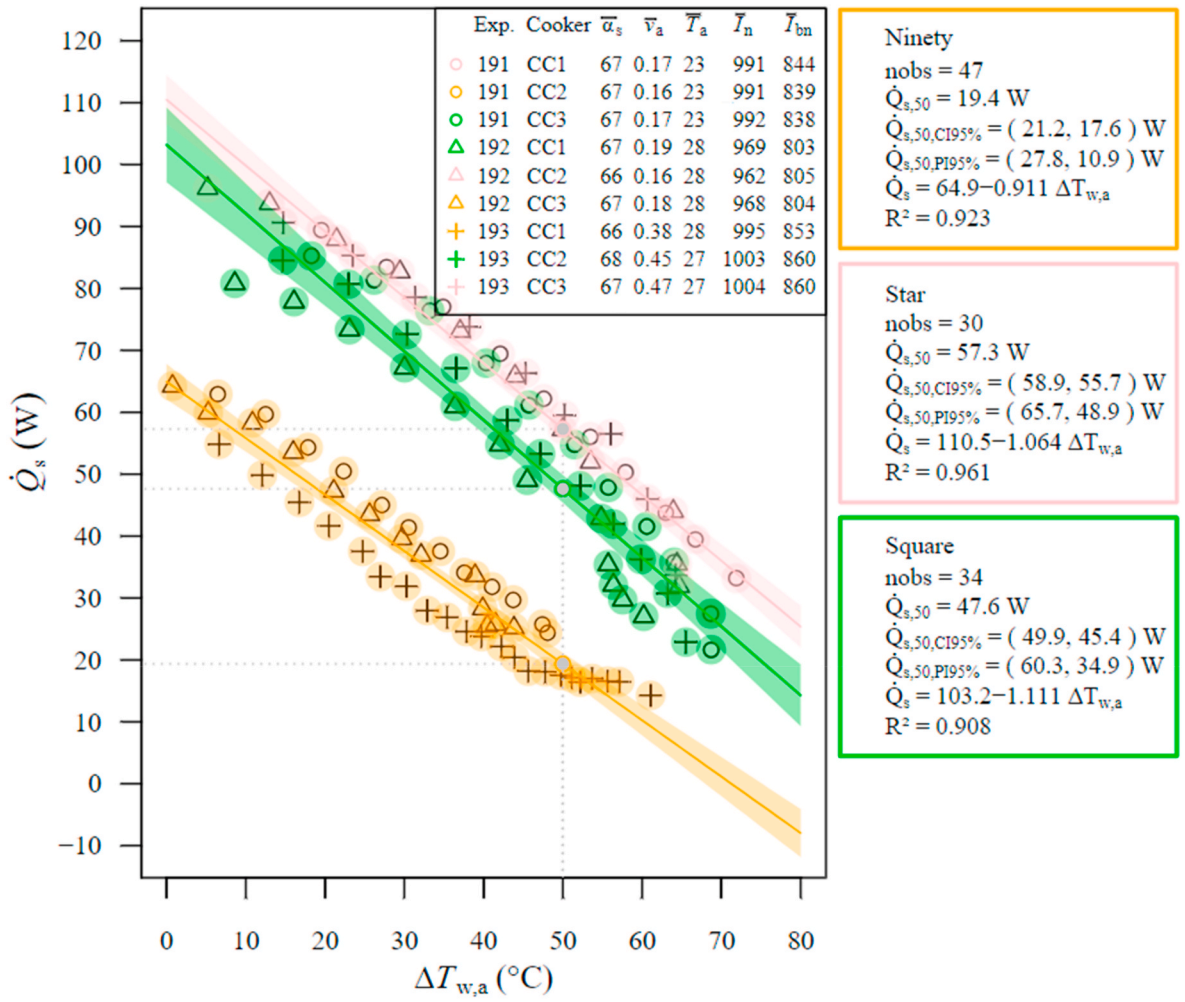

Fig. 9. Standardised power ($\dot{Q}_s$) vs. temperature difference ($\Delta T_{w,a}$) for medium average solar altitude angle ($66° \leq \overline{\alpha}_s \leq 68°$) for the *Ninety*, *Star* and *Square* configurations.

ranges. Similarly, new *Big*, new *Medium* and original *Flower* configurations perform better for high solar altitude angles. It is worth noting here that both groups were tested simultaneously ensuring comparability.

Fig. 7 shows performance results of the best original configuration and best new configuration for each solar altitude angle. It also shows the differences in terms of difference of normalised temperature differences between the best original configuration and the best new configuration ($\Delta T_{stag,s,new,original} = \Delta T_{stag,s,new} - \Delta T_{stag,s,original}$). For solar altitude angles below 35°, the temperature difference $\Delta T_{stag,s,new,original}$ remains below 10 °C, since the *Square* configuration performs slightly better than the *Ninety*. On average, an increase of 5.3 °C (9.6 %) is achieved for $\Delta T_{stag,s,new,original}$. For the range $35° < \alpha_s \leq 70°$, the *Star* shows an average increase of 23.9 °C (29.1 %) in $\Delta T_{stag,s,new,original}$, with a maximum of 31.6 °C at $\alpha_s = 55°$ compared to the *Ninety*. Last, in the high solar altitude angle range ($\alpha_s > 70°$), the largest difference of $\Delta T_{stag,s,new,original}$ is observed. The *Big Flower* provides a $\Delta T_{stag,s,new,original}$ increases of 34.7 °C (41.7 %) on average almost doubling the performance of the original *Flower*. Overall, the new configurations significantly increase the standardised stagnation temperature difference $\Delta T_{stag,s}$, i.e., the ratio of optical efficiency to heat loss factor, which is a promising result that must be further validated through water heating tests. More information on the parameters used for each test can be consulted in Table A1 in Appendix A.

4.2. Results of tests with load

Water heating tests are conducted simultaneously for the *Ninety*, *Star* and *Square* configurations, for testing periods with average solar altitude angles ($\overline{\alpha}_s$) of 35° (Fig. 8) and 66° (Fig. 9) while the *Flower* configurations are tested for 75° (Fig. 10). In the legend of Figs. 8 and 9, CC1, CC2 and CC3 is a code that corresponds to the cooker tested in each experiment, respectively, original *Ninety*, new *Star* and new *Square*. In the legend of Fig. 10, CC1, CC2 and CC3 is a code that corresponds to the cooker tested in each experiment, respectively, original *Flower*, new Medium *Flower,* and new *Big Flower*.

For low average solar altitude angle, (Fig. 8), the standardised power $\dot{Q}_{s,50}$ of the *Square* configuration is the greatest (48.4 W) showing an improvement of around 10 W compared to the original *Ninety* configuration (38.5 W). This is consistent with the results of the stagnation tests (Fig. 7). On the other hand, the power value $\dot{Q}_{s,50}$ of the new *Star* configuration performance is much lower (28.9 W), so it is not adequate in this range of solar altitude angle.

Another relevant observation from Fig. 8, is that the trend of the plotted standard power points somewhat deviates from the linear pattern. However, the R^2 (coefficient of determination) is always around 0.9 which is a reasonable value for a linear regression.

Analysing Fig. 9 for medium average values of solar altitude angle ($66° \leq \overline{\alpha}_s \leq 68°$), the *Star* configuration shows the greatest standard power $\dot{Q}_{s,50}$ (57.3 W), being almost 10 W higher than that from the

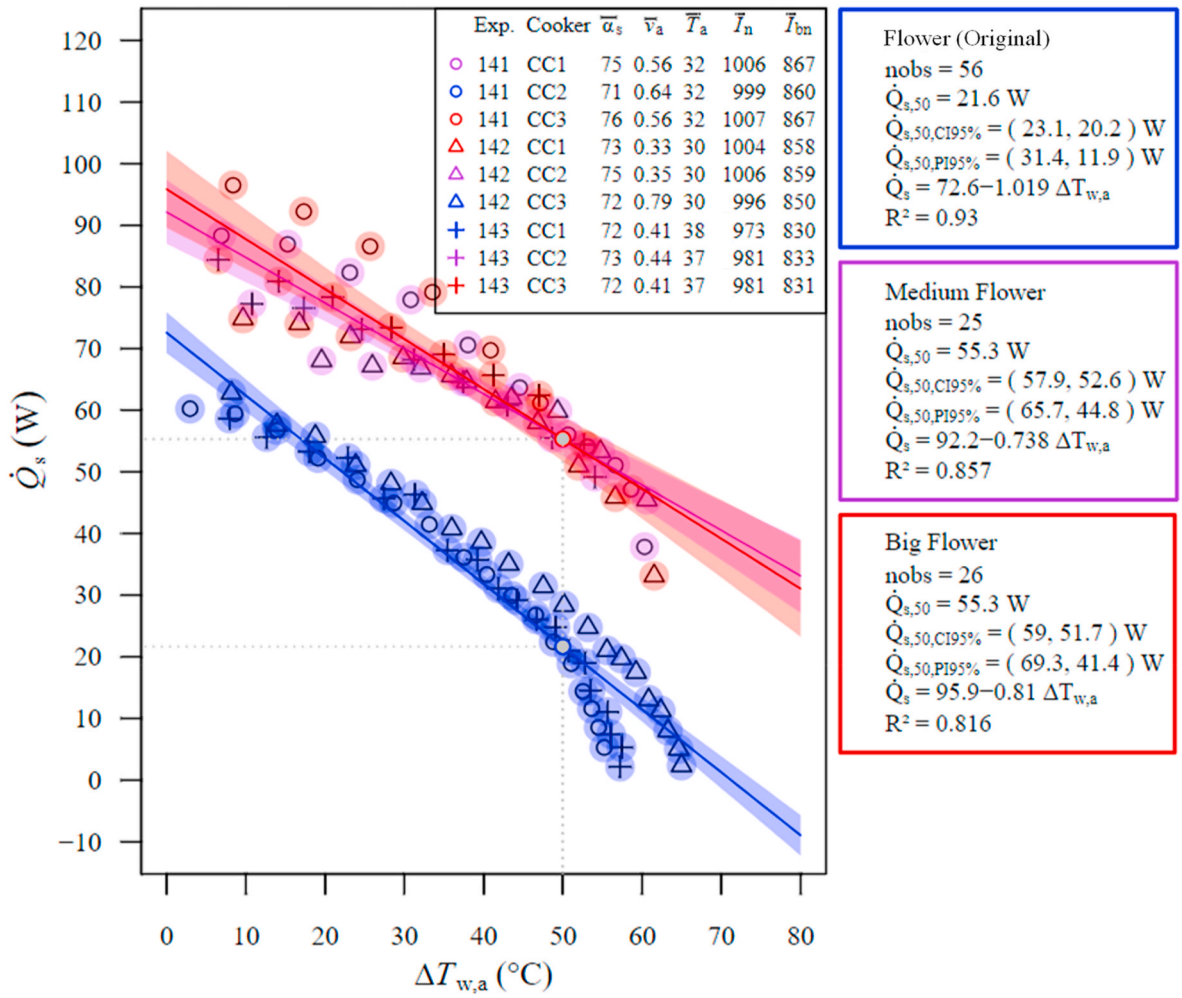

Fig. 10. Standardised power ($\dot{Q}_s$) vs. temperature difference ($\Delta T_{w,a}$) for high average solar altitude angle ($71° \leq \overline{\alpha}_s \leq 76°$), for the *Flower*, *Medium Flower* and *Big Flower* configurations.

Table 3
Summary of the key performance indicators for the configurations.

				Tests with load					Tests without load	
$\overline{\alpha}_s$ (°)	Configuration	$A_{n,max}$ (m^2)	$\Delta A_{n,max,new,original}$ (%)	$\dot{Q}_{S,50}$ (W)	η_{50} (–)	$\dot{Q}_{S,0}$ (W)	$\Delta \dot{Q}_{s,0,new,original}$ (W)	$\Delta \dot{Q}_{s,50,new,original}$ (W)	$\Delta T_{s,stag}$ (°C)	$\Delta T_{s,stag,new,original}$ (°C)
High 72–75	*Flower* (original)	0.197	–	21.6	10.6	72.6	–	–	77.3	–
	Medium Flower (new)	0.320	62.4	55.3	17.3	92.2	19.6	33.7	102.6	25.3
	Big Flower (new)	0.401	103.6	55.3	13.8	95.9	23.3	33.7	107.8	30.5
Medium 66–68	*Ninety* (original)	0.238	–	19.4	7.9	64.9	–	–	76.1	–
	Star (new)	0.317	33.2	57.3	17.8	110.5	45.6	37.9	103.9	27.8
	Square	0.339	42.4	47.6	13.9	103.2	38.3	28.2	79.7	3.6
Low 34–35	*Ninety* (original)	0.238	–	38.5	14.8	94.4	–	–	78.1	–
	Star (new)	0.317	33.2	28.9	8.2	78.3	−16.1	−9.6	85.3	7.2
	Square (new)	0.339	42.4	48.4	13.5	102.6	8.2	9.9	86.9	8.8

Square (47.6 W) and representing an impressive improvement of 38 W over the original Ninety configuration (19.4 W). These results are again consistent with those of the stagnation tests (Fig. 7).

Last, in the case of high average solar altitude angles ($71° \leq \overline{\alpha}_s \leq 76°$), Fig. 10, the two new configurations provide higher power than the original *Flower* and both show similar behaviour. *Medium* and *Big Flower* yield a power value of 55.3 W, i.e., when compared with 21.6 W from the original *Flower*, an increase of 33.7 W is evident. This is in line with the results of the stagnation tests (Fig. 7), which provided increases of normalised temperature differences between 25.3 °C and 30.5 °C for the *Medium* and *Big Flower* respectively.

A summary of the results obtained in the water heating tests and stagnation tests is presented in Table 3. For each solar altitude angle range, there is, at least, one new configuration that increases the standardised power over the original configuration. To guarantee a standardised power value above 48 W, the *Square* should be used for low solar altitude angle, the *Star* for medium solar altitude angle and the *Medium Flower* or *Big Flower* for high solar altitude angle.

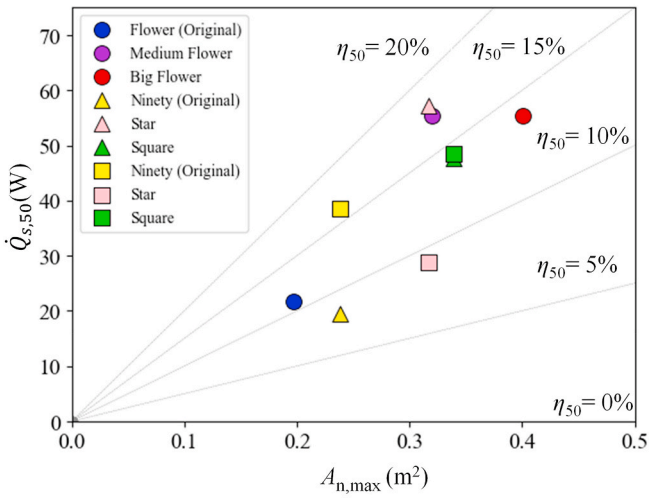

Fig. 11. Performance of the best configurations for high (circle), medium (triangle) and low (square) solar altitude angles.

To close this section, the points defined by standardised power $\dot{Q}_{s,50}$ and the aperture area $A_{n,max}$ for the different cooker configurations are represented in Fig. 11. In the same figure, the isolines of efficiency values η_{50}, i.e., values of efficiency for $\Delta T_{w,a} = 50$ °C are also represented. It can be observed that the *Star* configuration for medium solar altitude angles and the *Medium Flower* for high solar altitude angles show the highest efficiency η_{50} values of 18.1 % and 17.3 %. Yet, from a practical point of view, the most relevant result is the power provided rather than the efficiency since the latter is subject to the aperture area. It is important to point out that the tested configurations have different aperture areas, but the four reflectors of each configuration have the same dimensions and the same characteristics.

To further illustrate the benefits of the new configurations not only in terms of power or performance but on the dynamics of the experiment, the *Star* configuration under medium solar altitude angle conditions required less than 2 h (114 min) to bring 1.5 kg of water to its boiling point while the *Ninety* required 4 h (experiment 193). This result is of extreme relevance for real cooking applications. More information on this and the rest of the experiments can be found in Table A2 in Appendix A.

5. Conclusions

New configurations for the Copenhagen solar cooker are proposed. They differ from each other in the connection points between sheets, which means that they do not require additional resources to be implemented. These new configurations were tested simultaneously with water loads for periods with average solar altitude angles representing low (35°), medium (66°) and high (75°). For low solar altitude angles, using the new proposed Square configuration leads to a 25 % improvement in power $\dot{Q}_{s,50}$ over the original *Ninety* configuration. In the case of medium and high solar altitude angles, using the new proposed *Star*, *Medium Flower* and *Big Flower* configurations leads to an impressive 150 % improvement in power $\dot{Q}_{s,50}$ over the original *Ninety* and *Flower* configurations.

The stagnation tests without load qualitatively provide similar results to the water load tests. The stagnation tests, which are faster than the water heating tests, are good predictors for the behaviour of the cooker with loads for a given solar altitude angle, which is a piece of information of great importance for solar cooker users. However, more research is required to develop a quantitative, accurate, correlation between stagnation tests and water heating tests.

The performance improvement of the new proposed configurations can be largely attributed to the increase in the aperture area. As an example, the *Big Flower* implies an area increase of 103 % and a normalised power of 156 % compared to the original *Flower*.

Based on the results presented in this work, it is recommended that the *Square* configuration is adopted for solar altitude angle below 35°, the *Star* for solar altitude angles between 35° and 70° and, finally, the *Big/Medium Flower* for solar altitude angles above 70°.

In future work, the authors would like to investigate how results of tests without load could be used to predict the performance of solar cookers with loads. In present work, the authors have only examined this question using a qualitative approach.

CRediT authorship contribution statement

Xabier Apaolaza-Pagoaga: Writing – review & editing, Writing – original draft, Visualization, Supervision, Methodology, Investigation, Formal analysis, Data curation, Conceptualization. **Antonio Carrillo-Andrés:** Writing – review & editing, Visualization, Software, Methodology, Formal analysis, Data curation. **Juan-Pablo Jiménez-Navarro:** Writing – review & editing, Writing – original draft, Visualization, Methodology, Data curation. **Celestino Rodrigues Ruivo:** Writing – review & editing, Methodology, Formal analysis, Conceptualization.

Declaration of competing interest

The authors declare that they have no known competing financial interests or personal relationships that could have appeared to influence the work reported in this paper.

Acknowledgements

The authors would like to acknowledge Mr. Dave Oxford, of SLiCK solar stove UK, for suggesting the *Square* configuration that has been tested in this study. The authors would also like to acknowledge Mrs. Sharon Clausson for providing the Copenhagen solar cookers used in this work.

Appendix A. Data of all tests conducted in the present study

Tables A1 to A2 summarize the data of tests without load performed with different cooker configurations and Tables A3 to A5 summarize the data of load heating tests. The variable time is written in terms of solar time.

Table A1
Data of testing original *Flower*, *Medium Flower* and *Big Flower* cooker configurations without load.

Expt. No.	197	198	209	216
Start time	6:46	7:06	7:30	6:37
End time	12:26	16:06	14:30	13:57
Date	May 17, 2022	May 18, 2022	Jun 24, 2022	Jul 14, 2022

(*continued on next page*)

Table A1 (*continued*)

Expt. No.	197	198	209	216
β (°)	0	0	+15	+15
$\bar{I}_n$ (W m^{-2})	933	882	952	885
$\bar{I}_{bn}$ (W m^{-2})	810	710	798	710
$\alpha_{s,start}$ (°)	20.3	24.4	31.3	19.9
$\alpha_{s,noon}$ (°)	72.5	72.7	76.7	75.0
$\alpha_{s,end}$ (°)	71.6	34.1	55.2	60.7
$\overline{T}_a$ (°C)	28	29	34	32
$\bar{v}_a$ (m s^{-1})	0.44	0.58	0.03	0.56

Table A2
Data of testing *Ninety*, *Square* and Star cooker configurations without load.

Expt. No.	210	211	213	215
Start time	6:50	6:45	6:40	6:57
End time	14:10	12:40	14:00	13:57
Date	Jun 30, 2022	Jul 1, 2022	Jul 6, 2022	Jul 13, 2022
β (°)	−20	−20	−20	+20
$\bar{I}_n$ (W m^{-2})	940	903	917	884
$\bar{I}_{bn}$ (W m^{-2})	779	716	742	681
$\alpha_{s,start}$ (°)	23.0	22.0	20.6	23.9
$\alpha_{s,noon}$ (°)	76.5	76.4	76.0	75.2
$\alpha_{s,end}$ (°)	59.2	74.1	61.0	60.8
$\overline{T}_a$ (°C)	30	26	29	31
$\bar{v}_a$ (m s^{-1})	0.70	1.30	0.64	0.46

Table A3
Data of testing original *Flower*, *Medium Flower* and *Big Flower* cooker configurations with load.

Expt. No.	141			142			143		
Cooker	*Medium Flower*	*Flower*	*Big Flower*	*Big Flower*	*Medium Flower*	*Flower*	*Flower*	*Medium Flower*	*Big Flower*
Start time	11:09	11:09	11:09	10:24	10:24	10:24	10:24	10:24	10:24
End time	12:53	14:00	12:50	12:22	12:22	13:59	14:00	12:12	12:13
Date	Jun 29, 2021	Jun 29, 2021	Jun 29, 2021	Jul 2, 2021	Jul 2, 2021	Jul 2, 2021	Jul 6, 2021	Jul 6, 2021	Jul 6, 2021
m_w (kg)	1.5	1.5	1.5	1.5	1.5	1.5	1.5	1.5	1.5
n_p	9	17	8	10	8	20	19	8	8
$\bar{I}_n$ (W m^{-2})	1006	999	1007	1004	1006	996	973	981	981
$\bar{I}_{bn}$ (W m^{-2})	867	860	867	858	859	850	830	833	831
$\overline{\alpha}_s$ (°)	75	71	76	73	75	72	72	73	72
$\alpha_{s,start}$ (°)	72.6	72.6	72.6	65.1	65.1	65.1	64.8	64.8	64.8
$\alpha_{s,noon}$ (°)	76.5	76.5	76.5	76.4	76.4	76.4	76.0	76.0	76.0
$\alpha_{s,end}$ (°)	72.3	59.2	73.1	75.6	75.6	61.1	61.0	75.8	75.8
$\overline{T}_a$ (°C)	32	32	32	30	30	30	38	37	37
$\bar{v}_a$ (m s^{-1})	0.56	0.64	0.56	0.33	0.35	0.79	0.41	0.44	0.41
$\dot{Q}_{S,50}$ (W)	55.9	19.2	58.6	51.1	56.1	24.9	19.3	54.8	59.2
R^2	0.930	0.942	0.975	0.885	0.844	0.968	0.938	0.960	0.975

Table A4
Data of testing *Ninety*, *Square* and *Star* cooker configurations with load.

Expt. No.	161			162			163		
Cooker	*Ninety*	*Star*	*Square*	*Star*	*Square*	*Ninety*	*Square*	*Ninety*	*Star*
Start time	10:00	10:00	10:00	10:28	10:28	10:28	10:28	10:28	10:28
End time	14:00	14:00	13:12	13:28	12:44	13:28	12:55	13:34	13:58
Date	Nov 8, 2021	Nov 8, 2021	Nov 8, 2021	Nov 9, 2021	Nov 9, 2021	Nov 9, 2021	Nov 10, 2021	Nov 10, 2021	Nov 10, 2021
m_w (kg)	1.5	1.5	1.5	1.5	1.5	1.5	1.5	1.5	1.5
$\bar{I}_n$ (W m^{-2})	960	960	966	938	941	935	937	938	937
$\bar{I}_{bn}$ (W m^{-2})	883	883	892	860	864	858	857	857	855
$\overline{\alpha}_s$ (°)	35	35	35	35	35	34	35	35	34
$\alpha_{s,start}$ (°)	29.6	29.6	29.6	29.3	29.3	29.3	29.1	29.1	29.1
$\alpha_{s,noon}$ (°)	36.8	36.8	36.8	36.5	36.5	36.5	36.3	36.3	36.3
$\alpha_{s,end}$ (°)	29.4	29.4	34.2	29.7	35.5	29.7	34.7	31.8	29.5
$\overline{T}_a$ (°C)	22	22	21	22	22	22	21	21	21
$\bar{v}_a$ (m s^{-1})	0.11	0.11	0.02	0.04	0.02	0.04	0.56	0.57	0.59

(*continued on next page*)

Table A4 (*continued*)

Expt. No.	161			162			163		
Cooker	*Ninety*	*Star*	*Square*	*Star*	*Square*	*Ninety*	*Square*	*Ninety*	*Star*
$\dot{Q}_{S,50}$ (W)	34.3	27.8	46.4	28.3	52.2	41.3	48.2	40.8	30.9
R^2	0.950	0.942	0.918	0.855	0.911	0.930	0.963	0.960	0.893

Table A5
-Data of testing *Ninety*, *Square* and *Star* cooker configurations with load.

Expt. No.	191			192			193		
Cooker	*Star*	*Ninety*	*Square*	*Square*	*Star*	*Ninety*	*Ninety*	*Square*	*Star*
Start time	10:15	10:15	10:15	10:05	10:05	10:05	10:05	10:05	10:05
End time	12:17	13:00	13:00	12:45	12:11	12:45	14:05	12:16	11:59
Date	May 5, 2022	May 5, 2022	May 5, 2022	May 6, 2022	May 6, 2022	May 6, 2022	May 9, 2022	May 9, 2022	9 May 2022
m_w (kg)	1.5	1.5	1.5	1.5	1.5	1.5	1.5	1.5	1.5
n_p	10	12	11	12	11	13	22	11	9
$\bar{I}_n$ (W m^{-2})	991	991	992	969	962	968	995	1003	1004
$\bar{I}_{bn}$ (W m^{-2})	844	839	838	803	805	804	853	860	860
$\bar{\alpha}_s$ (°)	67	67	67	67	66	67	66	68	67
$\alpha_{s,start}$ (°)	59.0	59.0	59.0	57.5	57.5	57.5	58.2	58.2	58.2
$\alpha_{s,noon}$ (°)	69.4	69.4	69.4	69.7	69.7	69.7	70.5	70.5	70.5
$\alpha_{s,end}$ (°)	69.1	65.4	65.4	67.3	69.5	67.3	56.2	70.2	70.5
$\bar{T}_a$ (°C)	23	23	23	28	28	28	28	27	27
$\bar{v}_a$ (m s^{-1})	0.17	0.16	0.17	0.19	0.16	0.18	0.38	0.45	0.47
$\dot{Q}_{S,50}$ (W)	58.8	23.2	52.7	42.4	55.4	19.6	18.0	48.0	57.9
R^2	0.994	0.997	0.965	0.959	0.960	0.982	0.957	0.974	0.943

Appendix B. Calculation of the solar irradiance on a tilted plane

The Liu Jordan isotropic sky model described in Ref. [18] was used for the calculation of the solar irradiance on a titled surface. This model considers three components of the solar radiation: beam, isotropic diffuse and solar radiation diffusely reflected from the surroundings (typically ground). Thus, circumsolar diffuse and horizon brightening components are neglected. Under these assumptions, the total solar irradiance on the titled surface to an arbitrary titled surface, I_T, is estimated by:

$$I_T = I_b R_b + I_d\left(\frac{1+cos\,\beta}{2}\right) + I\rho_g\left(\frac{1-\cos\beta}{2}\right) \tag{B.1}$$

where I_b is the beam irradiance measured on a horizontal surface, R_b is the ratio of beam radiation on the titled surface to that on a horizontal surface at any time, i.e., $R_b = \cos\theta/\cos\theta_z$, θ is the angle of incidence (angle between the beam radiation on a surface and the normal vector to that surface) and θ_z is the zenith angle (the angle between the vertical and the line to the sun). The solar altitude angle corresponds to $\alpha = 90 - \theta_z$. Moreover, I_d is the diffuse irradiance measured on a horizontal surface, I is the global irradiance on a horizontal surface ($I = I_b + I_d$), and ρ_g is the ground diffuse reflectance (albedo). Finally, $(1+\cos\beta)/2$ is the view factor to the sky of a surface titled at slope β from the horizontal and $(1-\cos\beta)/2$ is the view factor to the ground.

If the Liu Jordan model is applied to the case of a surface that is tracking the sun perfectly, then $\cos\theta = 1$ and $\beta = \theta_z$, hence:

$$I_n = \frac{I_b}{cos\,\theta_z} + I_d\left(\frac{1+cos\,\theta_z}{2}\right) + I\rho_g\left(\frac{1-\cos\theta_z}{2}\right) \tag{B.2}$$

where I_n is the global irradiance on the surface normal to the incoming beam solar radiation.

In this work, both I_b and I_d (and therefore) are measured by a Delta-T Devices SPN1 pyranometer. This is a research-grade device that uses an array of thermopile sensors and a computer-generated shading pattern to measure the direct and diffuse components of incident solar radiation. On the other hand, $cos\,\theta_z$ is determined by the usual trigonometric formulation:

$$cos\,\theta_z = cos\,\varphi\cos\delta\cos\omega + \sin\varphi\,sin\,\delta \tag{B.3}$$

where φ is the latitude, δ is the declination, and ω is the hour angle (15° per hour, morning negative, afternoon positive). Thus, I_n can be readily determined for any instant.

Additionally to the use of Delta-T Devices SPN1, two more pyranometers (HukseFlux LP02) are used to measure global solar irradiance. They are located very close to the cookers. One LP02 sensor is placed on a horizontal plane, so it measures $I = I_b + I_d$. This measure is redundant with that of the Delta-T SPN1, so it serves as a verification. The other LP02 sensor is placed on a plane titled a slope $\beta = 40°$ from the horizontal and is adjusted manually to track the sun in azimuth. This sensor does not measure the global normal irradiance as the slope is not adjusted, and the resulting elevation angle is constantly 50°. This angle is an intermediate value between the solar altitude of the winter tests (around 30°) and that of the summer tests (around 70°). Global solar irradiance measurements of this sensor can be used as a reference to verify the calculations made with the Liu Jordan

model in this way: if the Liu Jordan model (with SPN1 data) is able to predict the LP02 measurements with good agreement, then it increases the confidence in the calculation of global normal irradiance, as the actual solar altitude angle during the tests will be not far from 50°. To predict the measurements of the LP02 with $\beta = 40°$, the angle of incidence is calculated as follows:

$$cos\ \theta = cos\ \theta_z \cos\beta + \sin\theta_z\ sin\ \beta \cos(\gamma_s - \gamma) \quad \text{(B.4)}$$

with $\beta = 40°$ and the difference between the azimuth angle of the sun, γ_s, and the azimuth of the solar cooker, γ, is assumed to be 0 ° approximately, as there is azimuthal tracking. Good agreement was found between the LP02 sensor measurements and the Liu Jordan model results, using the typical value for the ground diffuse reflectance $\rho_g = 0.2$.

References

[1] Eurostat, Energy consumption in households. https://ec.europa.eu/eurostat/databrowser/view/nrg_d_hhq/default/table?lang=en, 2022. (Accessed 15 May 2023).

[2] E. Cuce, P.M. Cuce, A comprehensive review on solar cookers, Appl. Energy 102 (2013) 1399–1421, https://doi.org/10.1016/J.APENERGY.2012.09.002.

[3] U.C. Arunachala, A. Kundapur, Cost-effective solar cookers: a global review, Sol. Energy 207 (2020) 903–916, https://doi.org/10.1016/j.solener.2020.07.026.

[4] X. Apaolaza-Pagoaga, A. Carrillo-Andrés, C.R. Ruivo, Experimental characterization of the thermal performance of the Haines 2 solar cooker, Energy 257 (2022), https://doi.org/10.1016/j.energy.2022.124730.

[5] G. Hebbar, S. Hegde, B. Sanketh, L.R. Sanith, R. Udupa, Design of solar cooker using evacuated tube solar collector with phase change material, Mater. Today Proc. 46 (2021) 2888–2893, https://doi.org/10.1016/J.MATPR.2021.03.629.

[6] M. Hosseinzadeh, A. Faezian, S.M. Mirzababaee, H. Zamani, Parametric analysis and optimization of a portable evacuated tube solar cooker, Energy 194 (2020) 116816, https://doi.org/10.1016/J.ENERGY.2019.116816.

[7] M. Noman, A. Wasim, M. Ali, M. Jahanzaib, S. Hussain, H.M.K. Ali, H.M. Ali, An investigation of a solar cooker with parabolic trough concentrator, Case Stud. Therm. Eng. 14 (2019) 100436, https://doi.org/10.1016/J.CSITE.2019.100436.

[8] X. Apaolaza-Pagoaga, A. Carrillo-Andrés, C. Rodrigues Ruivo, Experimental thermal performance evaluation of different configurations of Copenhagen solar cooker, Renew. Energy 184 (2022) 604–618, https://doi.org/10.1016/j.renene.2021.11.105.

[9] X. Apaolaza-Pagoaga, A. Carrillo-Andrés, C.R. Ruivo, New approach for analysing the effect of minor and major solar cooker design changes: influence of height trivet on the power of a funnel cooker, Renew. Energy 179 (2021) 2071–2085, https://doi.org/10.1016/j.renene.2021.08.025.

[10] X. Apaolaza-Pagoaga, A. Carrillo-Andrés, C.R. Ruivo, F. Fernández-Hernández, The effect of partial loads on the performance of a funnel solar cooker, Appl. Therm. Eng. 219 (2023), https://doi.org/10.1016/j.applthermaleng.2022.119643.

[11] X. Apaolaza-Pagoaga, A.A. Sagade, C. Rodrigues Ruivo, A. Carrillo-Andrés, Performance of solar funnel cookers using intermediate temperature test load under low sun elevation, Sol. Energy 225 (2021) 978–1000, https://doi.org/10.1016/j.solener.2021.08.006.

[12] B. Koshti, R. Dev, A. Bharti, A. Narayan, Comparative performance evaluation of modified solar cookers for subtropical climate conditions, Renew. Energy 209 (2023) 505–515, https://doi.org/10.1016/J.RENENE.2023.04.021.

[13] C.R. Ruivo, X. Apaolaza-Pagoaga, A. Carrillo-Andrés, G. Coccia, Influence of the aperture area on the performance of a solar funnel cooker operating at high sun elevations using glycerine as load, Sustain. Energy Technol. Assessments 53 (2022), https://doi.org/10.1016/j.seta.2022.102600.

[14] C.R. Ruivo, A. Carrillo-Andrés, X. Apaolaza-Pagoaga, Experimental determination of the standardised power of a solar funnel cooker for low sun elevations, Renew. Energy 170 (2021) 364–374, https://doi.org/10.1016/j.renene.2021.01.146.

[15] S.L. Clausson, A comparison of Copenhagen Solar Cookers with other similar sized solar cookers, in: CONSOLFOOD 2018 – International Conference on Advances in Solar Thermal Food Processing, Faro, Portugal, 2018.

[16] P. Arveson, Procedure for determining the intercept area of a solar cooker, SHE Technical Report no. TR-10 (2017), in: https://www.she-inc.org/wp-content/uploads/2018/04/TR-10-Procedure-for-Determination-of-the-Intercept-Area-of-a-Solar-Cooker.pdf (accessed November 21, 2023).

[17] American Society of Agricultural and Biological Engineers, ASAE S580.1 Testing and Reporting Solar Cooker Performance, 2013.

[18] J.A.B.W.A. Duffie, W.A. Beckman, Solar Engineering of Thermal Processes, John Wiley & Sons, Inc., Hoboken, NJ, USA, 2013, https://doi.org/10.1002/9781118671603.

[19] C.R. Ruivo, G. Coccia, G. Di Nicola, A. Carrillo-Andrés, X. Apaolaza-Pagoaga, Standardised power of solar cookers with a linear performance curve following the Hottel-Whillier-Bliss formulation, Renew. Energy 200 (2022) 1202–1210, https://doi.org/10.1016/j.renene.2022.10.041.

[20] S.C. Mullick, T.C. Kandpal, A.K. Saxena, Thermal test procedure for box-type solar cookers, Sol. Energy 39 (1987) 353–360, https://doi.org/10.1016/S0038-092X(87)80021-X.